

Bloch-band picture for light-pulse atom diffraction and interferometry

Daniel Gochnauer,¹ Katherine E. McAlpine,¹ Benjamin Plotkin-Swing,¹ Alan O. Jamison,² and Subhadeep Gupta¹

¹*Department of Physics, University of Washington, Seattle, Washington 98195, USA*

²*Department of Physics and MIT-Harvard Center for Ultracold Atoms, Research Laboratory of Electronics, Massachusetts Institute of Technology, Cambridge, Massachusetts 02139, USA*



(Received 21 June 2019; published 21 October 2019)

We apply a Bloch-band approach to the analysis of pulsed optical standing wave diffractive elements in optics and interferometry with ultracold atoms. We verify our method by comparison to a series of experiments with Bose-Einstein condensates. The approach provides accurate Rabi frequencies for diffraction pulses and is particularly useful for the analysis and control of diffraction phases, an important systematic effect in precision atom interferometry. Utilizing this picture, we also demonstrate a method to determine atomic band structure in an optical lattice through a measurement of phase shifts in an atomic contrast interferometer.

DOI: [10.1103/PhysRevA.100.043611](https://doi.org/10.1103/PhysRevA.100.043611)

I. INTRODUCTION

The motion of electrons in the periodic potential of ionic crystals is addressable by the celebrated Bloch solutions which give rise to band structure [1,2]. Periodic potentials are also common in the arena of ultracold atoms where gases trapped in optical lattices can serve as a test bed for questions in many-body physics [3–5]. These scenarios are amenable to the same band-structure approach.

Pulsed optical lattices are in common use as diffractive elements in atom optics and interferometry [6] for diverse applications such as inertial sensing [7–10] and for tests of fundamental physics such as the equivalence principle [11–13] and quantum electrodynamics [14,15]. The atom-optics element of choice for beam splitters and mirrors—Bragg diffraction—is traditionally analyzed using the two-state Rabi solution which predicts oscillatory behavior [16,17]. To address the regime when the two-state approximation is invalidated for sufficiently short pulses, a host of numerical work has been performed [18–20] with the limiting case of Kapitza-Dirac diffraction allowing an analytic solution [17].

In this work we apply the Bloch-band approach to atom optics through the performance and analysis of a series of standing-wave diffraction and interferometry experiments with Bose-Einstein condensates. Our results impact three key directions. First, we experimentally demonstrate the equivalence between the band gap and the frequency for Bragg pendellösung, and obtain accurate values distinct from the results of a commonly used formula for Rabi frequency in Bragg diffraction. Second, we exploit the Bloch-band approach for direct visualization and systematic analysis of diffraction phase effects and provide useful methods for their suppression in precision atom interferometry. Finally, we invert the approach and determine atomic band structure in a periodic potential from measurements of phase shifts in an atom interferometer, thus introducing a method for analyzing arbitrary periodic optical potentials.

II. ATOM OPTICS IN THE BLOCH-BAND PICTURE

Our analysis is based on the Bloch solutions for a neutral atom interacting with the one-dimensional sinusoidal potential of an optical standing wave and is related to earlier theoretical work [21,22]. In accord with parameters used in typical experiments, we work in a regime where the large one-photon detuning allows adiabatic elimination of the excited internal state. The atom-light interaction then reduces to a conservative (ac Stark shift) potential imposed on the atoms, which is proportional to the optical intensity [17]. We calculate the Bloch energy bands (Fig. 1) by numerically diagonalizing the single-particle Hamiltonian for the potential $U = U_0 \sin^2(2kx)$. The energy and momentum are normalized to the recoil energy $E_{\text{rec}} = \hbar^2 k^2 / 2m$ and recoil momentum $p_{\text{rec}} = \hbar k$, respectively, where π/k is the spatial periodicity of the lattice.

In a Brillouin-zone picture, the lattice opens up an avoided crossing at every intersection of free-particle energy levels, each of which can be identified with a Bragg diffraction process and is characterized by an energy gap which increases monotonically with U_0 . This band gap is equivalent to $\hbar\Omega_R$, where Ω_R is the Rabi frequency for oscillations between the two Bragg-coupled states. In addition, there is also an energy shift $\hbar\Omega_D$ of the mean energy of the coupled states away from the original (unperturbed) crossing point. Both Ω_R and Ω_D can be seen as arising from “level repulsion” in second-order perturbation (see Fig. 1 inset).

We now turn to determining the Bragg diffraction amplitude and phase in this picture. We explicitly consider an N_B th-order Bragg transition which can be seen as a $2N_B$ photon process connecting states $| -N_B \hbar k \rangle$ and $| +N_B \hbar k \rangle$. Here even (odd) N_B corresponds to a crossing at the center (edge) of the Brillouin zone. In the band picture, the Bragg process is the behavior of an initially free particle state which is loaded into the lattice at the N_B th avoided crossing as an equal superposition of the N_B th and $(N_B - 1)$ th excited bands (Bloch states). During the $2N_B$ photon pulse the populations

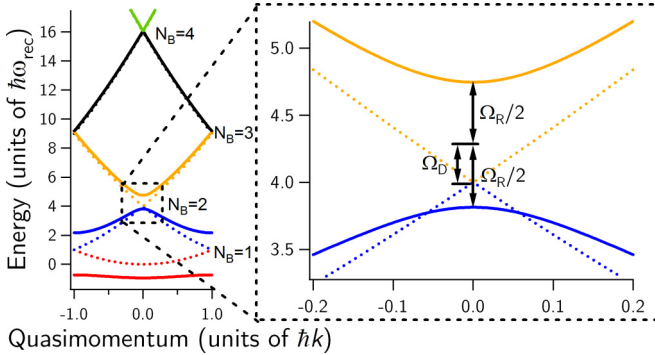


FIG. 1. Atomic energy bands in quasimomentum space for a sinusoidal optical lattice. Solid (dashed) lines are calculated with a depth, U_0 , of $6\hbar\omega_{\text{rec}}$ ($0\hbar\omega_{\text{rec}}$). The first- through fourth-order Bragg transitions are indicated by $N_B = 1\text{--}4$. The inset shows a close-up for $N_B = 2$. Ω_R and Ω_D correspond to the frequencies of Rabi flopping and diffraction phase evolution, respectively.

in the $|\pm N_B \hbar k\rangle$ states oscillate sinusoidally and out of phase with each other at angular frequency $\Omega_R(t)$. Since each of the $|\pm N_B \hbar k\rangle$ states spends equal time in each band, we may evaluate the corresponding phase by integrating the average energy of the two participating Bloch states, characterized by Ω_D , over the duration of the pulse. Within an atom interferometer, diffraction pulses are frequently applied to a superposition of free particle states separated in momenta by multiples of $2\hbar k$, corresponding to different interferometer paths. The different $\Omega_D(t)$ for different paths during these processes can then lead to an observable interferometer phase shift called the *diffraction phase*.

In order to apply the Bloch-band picture to pulsed standing waves, the time dependence of $U_0(t)$ must preserve the two-state nature of the Bragg process. Practically, the desire for high diffraction efficiency means experiments work in exactly this regime, showing the suitability of the Bloch-band approach.

For a time-varying standing-wave amplitude $U_0(t)$, adiabaticity mandates $\frac{1}{U_0} \frac{\partial U_0}{\partial t} \ll \Delta E/\hbar$, where ΔE is the energy separation from the eigenstate nearest to our two states of interest. Applying this criterion to the rise and fall times of a smooth (e.g., Gaussian) pulse shape with width τ , resonant with an N_B th-order Bragg process, we arrive at $\tau \gg \frac{1}{4N_B\omega_{\text{rec}}}$, where $\omega_{\text{rec}} = E_{\text{rec}}/\hbar$ is the recoil frequency. We recognize this inequality to be equivalent to being in the Bragg regime of diffraction where states other than $|\pm N_B \hbar k\rangle$ are not populated.

We compare the Bloch-band picture to both full numerical time evolution of the Schrödinger equation and experiments. In Bloch picture simulations, we numerically solve for the band structure at many different lattice depths. We then use these saved band structures to numerically integrate Ω_R and Ω_D for any given diffraction pulse profile to obtain population fraction and diffraction phase predictions. With a single set of band structures, the effects of any pulse shape or duration may be quickly calculated, allowing for rapid prototyping of experimental sequences. These simulations enforce adiabaticity by assuming the atoms' wavefunctions remain confined to the two bands corresponding to their free-space momenta. By contrast, full numerical evolution solves the time-dependent

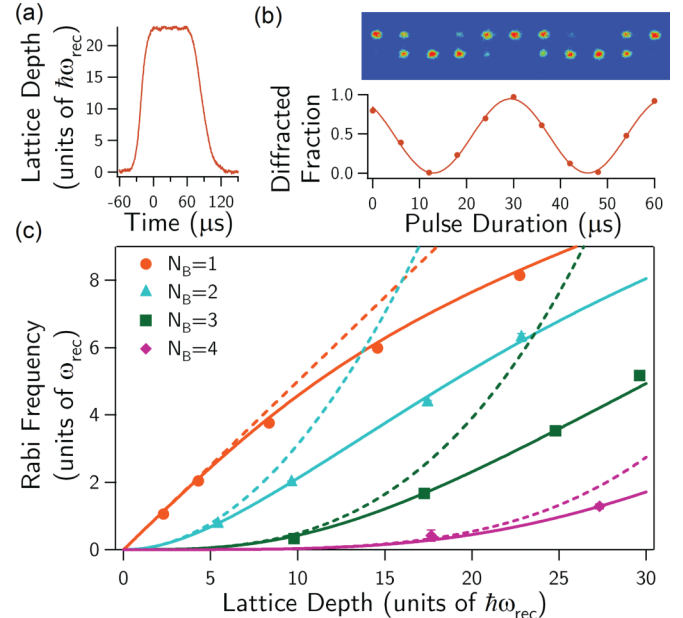


FIG. 2. Measurement of band gaps (Rabi frequencies). (a) Sample pulse profile. (b) Rabi oscillations for $N_B = 1$ in a $22.7\hbar\omega_{\text{rec}}$ lattice; upper panel shows corresponding sequence of time-of-flight absorption images. The pulse duration is defined as the extent of the intermediate flat region of the pulse profile. The diffracted fraction for zero pulse duration is due to the pulse rise and fall. (c) Measured Rabi frequency for various lattice depths and for $N_B = 1, 2, 3, 4$ (solid circles). Solid (dashed) lines are Bloch-band [right-hand side of Eq. (1)] predictions.

Schrödinger equation over a large basis of momentum states and uses the time evolution operator to extract population transfer and diffraction phase information (see Appendix B). A full time evolution must be calculated for every pulse shape or duration considered. Comparing to full time evolution allows us to quantify the nonadiabatic effects due to other bands missing from the adiabatic Bloch picture.

We test and verify the validity of the Bloch-band picture of atom optics in the $\tau \gtrsim \frac{1}{4N_B\omega_{\text{rec}}}$ “quasiadiabatic” regime (see Appendix A) and stay within the observed validity range for all the experimental work presented in this paper. Even when other states are negligibly populated, their presence has a significant effect for typical experimental parameters on both the splitting Ω_R and the shift Ω_D of the two coupled states. We now examine these effects individually.

III. ACCURATE RABI FREQUENCIES FOR BRAGG DIFFRACTION

We first report on our measurements of the Rabi frequency for various Bragg diffraction orders using a Bose-Einstein condensate (BEC) atom source. Our results experimentally establish the Bloch-band picture for atom optics and reveal the shortcomings of a commonly used result in the field (see Fig. 2).

The experiments reported in this work were carried out with BECs of 10^5 ytterbium (^{174}Yb) atoms. We prepared the BEC in a 532-nm crossed-beam optical dipole trap and released them from the confinement after reducing the mean

trap frequency to $\bar{\omega} = 2\pi \times 63$ Hz [23]. Upon release, the atoms are given 2 ms to expand before they encounter a diffraction pulse. The diffraction pulses are formed by a pair of horizontal, counterpropagating beams with a waist of 1.8 mm, blue detuned from the 556-nm intercombination line ($^1S_0 \rightarrow ^3P_1$) by $+3500\Gamma$, where $\Gamma = 2\pi \times 182$ kHz is the natural linewidth. The relative detuning between the two beams is controlled by direct digital synthesis electronics at the subhertz level. The size of the cloud during all the atom optics experiments is 34 μm , i.e., far less than the size of the diffraction beams. The depth of the optical lattice formed by these beams was calibrated with Kapitza-Dirac diffraction [17]. This method provided a depth calibration accurate at the $\pm 2\%$ level.

We applied diffraction pulses with temporal intensity profiles consisting of Gaussian rise and fall $1/e$ times of $\tau_{1/e} = 27 \mu\text{s}$ satisfying $4\omega_{\text{rec}}\tau_{1/e} = 2.5$, with an intermediate flat profile of variable extent [Fig. 2(a)]. The relative detuning δ of the lattice beams was set to match the Bragg resonance condition $\delta = 4N_B\omega_{\text{rec}}$. The population in each of the two coupled states was monitored by time-of-flight absorption imaging [Fig. 2(b), upper panel]. The fractional population in the final state oscillates as $P(t) = \sin^2[\frac{1}{2} \int_{t_0}^t \Omega_R^{(2N_B)}(t')dt']$, where $\Omega_R^{(2N_B)}$ is the Rabi frequency for an N_B th-order Bragg process [Fig. 2(b)]. As shown in Fig. 2(c), the measured $\Omega_R^{(2N_B)}$ is in good agreement with the Bloch-band calculation.

Figure 2(c) also demonstrates the inadequacy of a commonly used [17,24–26] generalized Rabi frequency formula first derived in [16], given by the right-hand side (RHS) of the inequality below:

$$\Omega_R^{(2N_B)} < \frac{[\omega_R]^{2N_B}}{2^{4N_B-3}[(N_B-1)!]^2 \Delta^{N_B} \omega_{\text{rec}}^{N_B-1}}. \quad (1)$$

Here ω_R is the single-photon Rabi frequency and Δ is the detuning from the excited state. The RHS is a perturbative result and therefore breaks down at large lattice depth, deviating significantly from the measured values. It is important to note that the standard pulse parameters used in Bragg diffraction experiments are comfortably outside this perturbative regime, stemming from the favoring of short pulses in experiments in order to minimize state manipulation time in comparison to the longer interferometer interaction times.

IV. APPLICATION TO DIFFRACTION PHASES IN ATOM INTERFEROMETRY

The Bloch-band picture allows a straightforward understanding and assessment of diffraction phases in atom interferometry. In addition to the $\hbar\Omega_R$ band gap, the perturbation of the lattice produces a shift $\hbar\Omega_D$ of the mean energy of the two coupled states [Fig. 1(b)]. In the presence of a lattice of depth U_0 , a particular path within an interferometer is characterized by a particular band number and quasimomentum q , accumulating an additional phase during a diffraction process:

$$\Phi_D = \frac{1}{\hbar} \int_{\text{pulse}} (\bar{E}(q, U_0) - E_f(q)) dt, \quad (2)$$

where E_f is the free-particle energy. For an interferometer path at Bragg resonance during the pulse, $\bar{E}(t) = E_f +$

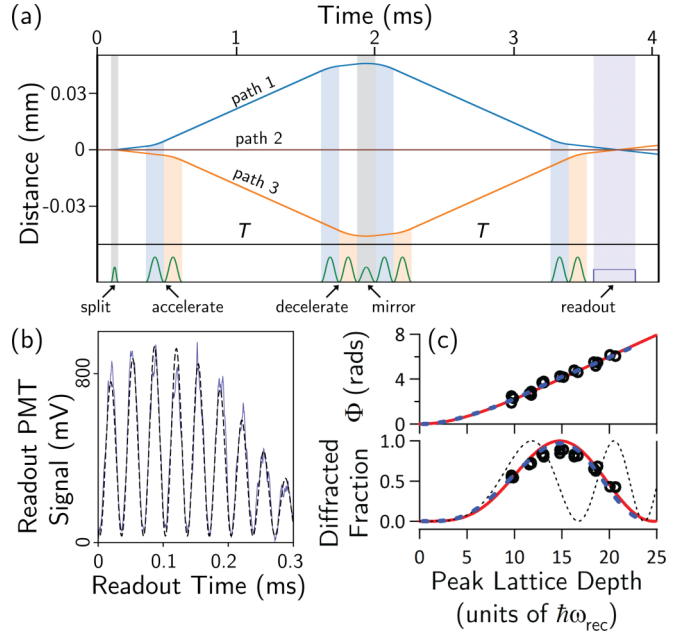


FIG. 3. (a) Space-time diagram for a CI with up to $16\hbar k$ momentum separation between the outer paths and free evolution time, $T = 1$ ms. (b) Representative readout signal for the CI (20-shot average) together with fitted sinusoid with a Gaussian envelope. (c) Varying the peak lattice depth of the mirror pulse changes both the diffracted fraction and the CI phase Φ . The solid red lines show the corresponding Bloch-band analysis predictions while the blue dashed lines show the full numerical integration theory, with both methods displaying good agreement with the data (open circles). The black dotted line is the prediction from the RHS of Eq. (1).

$\hbar\Omega_D(t)$; however, away from a Bragg resonance it is the energy of the band the path is loaded into. Bragg diffraction within an atom interferometer thus results in differential phase shifts between interferometer paths and can lead to an overall diffraction phase, with important ramifications for precision measurements [22,27,28].

We perform our experimental work on diffraction phases in a three-path contrast interferometer (CI) [see Fig. 3(a)] with a ^{174}Yb BEC source [23,27]. After release of our BEC from the trap, atoms are first placed in an equal superposition of three momentum-states ($|+2\hbar k\rangle$, $|0\hbar k\rangle$, $|-\hbar k\rangle$) using a short standing-wave light pulse operating in the Kapitza-Dirac regime [17]. The three parts of the wavefunction separate for time T after which the outer paths have their momenta reversed by a second-order Bragg π -pulse. The three paths are again spatially overlapped after an additional time T . The contrast of the resulting matter-wave interference pattern is measured as the Bragg reflection signal of a traveling-wave light pulse. This readout signal [Fig. 3(b)] has the oscillating form

$$S(t) = C(t) \cos^2 \left(\frac{\phi_1(t) + \phi_3(t)}{2} - \phi_2(t) \right), \quad (3)$$

where ϕ_i is the phase accrued by path i and $C(t)$ is an envelope function determined by the coherence time of the condensate source [23]. $S(t)$ oscillates at $8\omega_{\text{rec}}$ and is sensitive to the kinetic energy differences between the interfering paths and

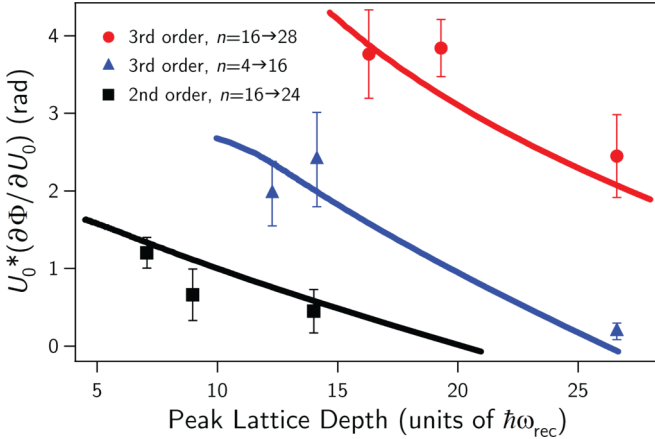


FIG. 4. Suppression of diffraction phase effects with pulse intensity. Measurements of $U_0 \partial \Phi / \partial U_0$ at the π -point for different Bragg acceleration pulses are in agreement with the Bloch-band calculation (curves). The pulses accelerated the outer paths from $|\pm 2\hbar k\rangle$ to $|\pm 8\hbar k\rangle$ (blue triangles), $|\pm 8\hbar k\rangle$ to $|\pm 12\hbar k\rangle$ (black squares), and $|\pm 8\hbar k\rangle$ to $|\pm 14\hbar k\rangle$ (red circles).

thus to the photon recoil frequency, and can therefore be used to precisely measure the fine structure constant [23]. We fit such signals with the expression $C(t_r) \cos^2(4\omega_{\text{rect}} t_r + \Phi) + S_0$, where t_r is the time from the start of the readout pulse and S_0 is a vertical offset. The momentum separation between outer paths during free evolution can be increased to $n\hbar k$ by the insertion of acceleration pulses [Fig. 3(a) shows $n = 16$] with the resulting CI phase $\Phi = \frac{1}{2}n^2\omega_{\text{rec}}T + \Phi_{\text{offset}}$. Diffraction phase effects are contained in Φ_{offset} , which we study by keeping T fixed and monitoring Φ for varying diffraction pulse parameters. All acceleration pulses used in this work are either second- or third-order Bragg pulses with Gaussian-shaped temporal profiles and are incorporated into the theoretical model as integrals over a time-varying $U_0(t)$ in Eq. (2).

As shown in Fig. 3(c) for the Bragg (second-order) mirror pulse, both the observed phase and the population oscillation are captured well by the Bloch-band model. While paths 1 and 3 acquire diffraction phase according to $N_B = 2$, path 2 remains in the lowest band. The observed subunity diffraction efficiency at the π -point (where the π -pulse condition is met) is due to the small but finite velocity width of the sample, which is not included in the model.

Since interferometry experiments are sensitive to diffraction phase through intensity noise (i.e., shot-to-shot variations in U_0), we characterize its effect using the measured quantity $U_0 \partial \Phi / \partial U_0$ at operating conditions, which for the CI geometry are π -pulses for both mirror and acceleration optics. This quantity serves as a good figure of merit for the typical situation where the uncertainty in depth scales with U_0 , since it normalizes the phase fluctuations at each depth. From data sets similar to Fig. 3(c), we determine the slopes at these π -points for several different pulse parameters of second- and third-order Bragg acceleration pulses (see Fig. 4) and find good agreement with the Bloch-band theory. When the momentum separation between the paths is large compared to recoil (i.e., multiband separation), this quantity becomes negligible except for the path(s) undergoing the Bragg transition.

Our analysis of diffraction phases in the Bloch-band picture shows that Ω_D / Ω_R monotonically decreases with lattice depth in Bragg diffraction for $N_B > 1$ [see Fig. 7(b) in Appendix C]. This is the reason for the observed decrease of $U_0 \partial \Phi / \partial U_0$ with increasing U_0 in Fig. 4.

This result points to an important consequence for precision interferometry: for high-order Bragg diffraction as commonly used for large-momentum-separation interferometers [23,29], diffraction phase effects are minimized by operating at as high a lattice depth as possible, as long as additional states are not populated by the process. This can be understood as the slowed growth of Ω_D with U_0 from the level repulsion of higher energy states (see Appendix C). Another result of our analysis is that the diffraction phase can be significantly modified by the presence of other interferometer paths in a nearby band [see Eq. (3)] as can be seen in the difference between the red and blue data points in Fig. 4. This method can be used to greatly suppress the diffraction phase effect (see blue data point at 27 recoils in Fig. 4). We can also see that certain interferometer geometries are immune to diffraction phases from the symmetry of pulse application, e.g., the symmetric Mach-Zehnder. However, interferometers that measure the recoil phase accrued between paths are generally sensitive to diffraction phases [15,23,27,28].

V. DETERMINING BAND STRUCTURE FROM INTERFEROMETER PHASE

While the earlier discussion is mainly focused on the application of the Bloch-band picture at avoided crossings, the picture applies equally well to all other points in quasimomentum space. This approach to atom diffraction and interferometry can thus naturally lend itself as a tool to determine band structure due to some unknown periodic potential. The transient presence of some unknown optical lattice manifests as an interferometric phase shift with different interferometer paths evolving phase according to the band number and quasimomentum into which they map. By varying these quantities with the atom optical elements of the interferometer, the complete band structure due to the unknown potential can be determined.

A clean implementation of this tool is furnished in the CI, modified as shown in Fig. 5(a). For demonstration purposes we determine the ground band structure in a sinusoidal optical lattice with Gaussian temporal shape and $4\omega_{\text{rec}}\tau_{1/e} = 2.5$. The value of quasimomentum q in the standing-wave frame is chosen by precisely controlling the relative detuning of the counterpropagating lattice beams in the laboratory frame. During the pulse, the middle path is in the bottom band (band 0) and the outer paths are in bands 7 and 8. Diffraction phase accrued by the outer paths is negligible compared to that accrued by the middle path. Figure 5(b) shows the measured CI phase at $q = 0$ for various lattice depths, in good agreement with the band theory prediction [30]. As we vary q at a fixed depth, the measured CI phase converted to an energy shows the characteristic ground band dispersion [Fig. 5(c)].

The data presented in Fig. 5(c) were obtained through a series of experiments in which a nondiffracting lattice is applied within the interferometer at a time highlighted (red stripe) in Fig. 5(a). Because the relative detuning of the two

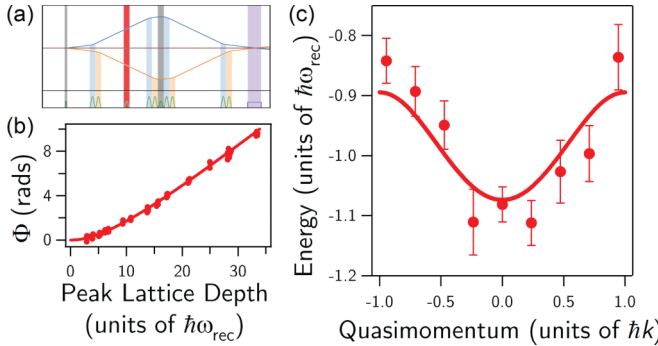


FIG. 5. (a) Space-time diagram for band structure measurement with a modified $n = 16$ CI. This is identical to Fig. 3(a) except for the additional pulsed lattice (dark red stripe) which imparts the band structure to be determined. (b) CI phase at $q = 0$ for various lattice strengths. (c) The ground band dispersion in a sinusoidal lattice from diffraction phase measurements. The solid line corresponds to the theoretical dispersion for a lattice depth of $6.5\hbar\omega_{\text{rec}}$.

lattice beams was chosen such that the middle interferometer path loaded into the bottom band, the other paths—having been accelerated—were loaded into much higher bands and thus contributed negligibly to the total CI phase. The quasimomentum q in the standing-wave frame could then be varied and any phase shift would be an observation of the lattice energy dispersion. The adiabaticity criterion prevents turning on a lattice at q near the Brillouin-zone edge without loading into a superposition of the bottom band and the first excited band. To measure the energy shift at a particular q value in only the bottom band, we developed the following procedure: First we adiabatically turned on a lattice at $q = 0$, reaching a depth of $6.5\hbar\omega_{\text{rec}}$ over $150\ \mu\text{s}$ with a cubic spline temporal shape. Next we linearly ramped the relative detuning between diffraction beams for $56\ \mu\text{s}$ until we reached $q = -0.95\hbar k$. Then we swept the relative detuning at the same rate in the opposite direction, stopping at the desired q for $100\ \mu\text{s}$, and eventually reaching $q = +0.95\hbar k$. Finally, the relative detuning was brought back to zero and the lattice turned off with the same cubic spline shape.

This method thus allowed us to directly measure the diffraction phase Φ_D as a function of quasimomentum. In accord with Eq. (2), we converted Φ_D to an energy shift and then added the calculated free-space energy at each q to obtain the ground band dispersion. In the experimental sequence the diffraction phase acquired during each intensity ramp and frequency ramp was common for all experimental iterations and resulted in a uniform offset phase in the experiment. This became an energy offset in the measured ground band dispersion, which we determined by fitting with one free parameter (the constant offset) to the calculated ground band energy dispersion for a $6.5\hbar\omega_{\text{rec}}$ -depth lattice. The obtained ground band dispersion determined from the data in this way shows good agreement with the theoretical calculation [Fig. 5(c)].

VI. DISCUSSION AND CONCLUSIONS

We have investigated a Bloch-band approach to analyzing atom diffraction and interferometry. Theoretical results for the

amplitude and phase associated with standing-wave diffraction show good agreement with measurements for arbitrary lattice strength. Significantly, our results span a range of atom optics parameters that extend beyond the weak lattice regime and are thus of practical importance for current atom interferometry experiments. While analytic formulas for diffraction amplitude are known from earlier work [16,17] and their inadequacy beyond the weak lattice limit is recognized [21,24], our results constitute an experimental study and its accurate analysis at arbitrary lattice depth. We have demonstrated the validity of a Bloch-band approach to diffraction phases by direct comparison to interferometric phase shifts. Our work also points out general methods to control diffraction phases, an important systematic effect in precision measurements. All our results, presented as scaled to recoil frequency and momentum, are generally valid for all atom diffraction and interferometry setups. Our interferometric method of band structure measurement is complementary to earlier methods [31,32] and, while demonstrated here only for the ground band, can be extended to excited bands as well by loading path 2 into the desired band. Furthermore, the method can also be adapted to nonsinusoidal periodic potentials, as well as to higher-dimensional and time-dependent (e.g., Floquet) lattices [33].

ACKNOWLEDGMENTS

We thank Tahiyat Rahman for experimental assistance. This work was supported by NSF Grant No. PHY-1707575 and by the NASA Fundamental Physics Program.

APPENDIX A: ADIABATICITY CRITERION

The potential from the time-varying diffraction pulse can be written as $U(x, t) = U_0(t)\sin^2(2kx)$. From the adiabatic theorem of quantum mechanics, we can write the adiabaticity criterion for a time-varying standing-wave amplitude $U_0(t)$ as

$$\frac{1}{U_0} \frac{\partial U_0}{\partial t} \ll \Delta E(q)/\hbar, \quad (\text{A1})$$

where $\Delta E(q)$ is the energy separation from the eigenstate nearest to our two states of interest. For the typical experimental situation of a pulse with smooth rise and fall times with width τ resonant with an N_B th-order Bragg process, the adiabatic criterion gives $\tau \gg \frac{1}{4(N_B-1)\omega_{\text{rec}}} \approx \frac{1}{4N_B\omega_{\text{rec}}}$ for $N_B > 1$, where $\omega_{\text{rec}} = E_{\text{rec}}/\hbar$ is the recoil frequency. For $N_B = 1$, $\tau \gg \frac{1}{8\omega_{\text{rec}}}$. The adiabatic criterion then is equivalent to being in the Bragg regime of diffraction where states other than the two coupled ones are not populated.

The Doppler width from the finite velocity spread Δv of the atomic source introduces another important timescale and the corresponding mandate of $\tau \ll \frac{1}{k\Delta v}$ is met by using subrecoil clouds of atoms. Additionally, practical considerations in atom optics applications put a premium on diffraction pulse times seeking to minimize this in favor of interferometer interaction times. It is thus critical to test the regime of validity of the Bloch-band picture of atom optics in the regime $\tau \gtrsim \frac{1}{4N_B\omega_{\text{rec}}}$, or a “quasiadiabatic” regime.

We perform this test by comparing the results for a Bragg π -pulse evaluated by the Bloch-band picture and a

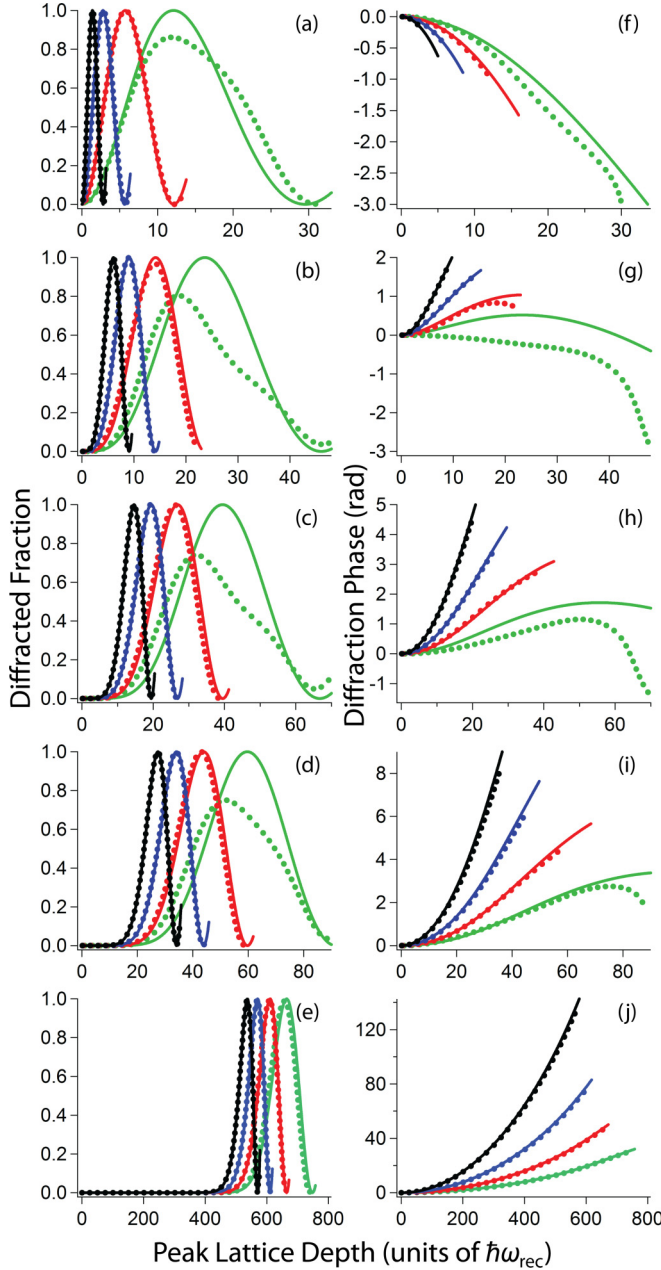


FIG. 6. (a–e) Diffracted fraction and (f–j) diffraction phase for $N_B = 1, 2, 3, 4$, and 16 Bragg processes. Each graph contains results for Gaussian pulses with $4\omega_{\text{rec}}\tau_{1/e} = 10.1, 5.04, 2.52$, and 1.26 . Solid lines show the result of the Bloch-band approach while the thick dashed lines show that of a full numerical integration in the free-particle basis. The two approaches maintain good agreement within the quasiadiabatic regime (see text). We note that the phase shift is common to the initial and the final states.

numerical integration of the problem in the free-particle basis, as described in earlier work [27] and summarized below. We use Gaussian pulses with different $1/e$ radii and observe (see Fig. 6) that the two calculations agree in both population and phase for timescales comfortably satisfying the adiabaticity criterion as well as into the quasiadiabatic regime convenient for and usually utilized in experiments. The signature of breakdown of the Bloch-band picture is simultaneous with

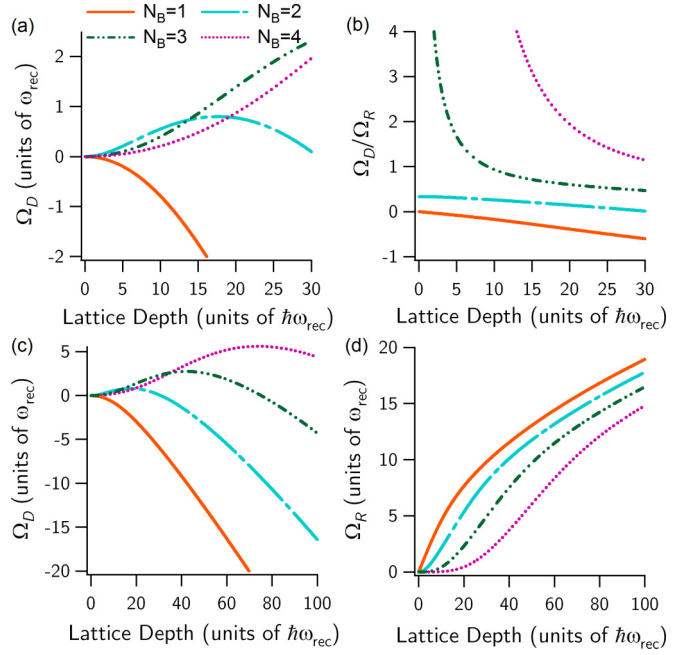


FIG. 7. (a) The frequency Ω_D associated with the diffraction phase plotted as a function of lattice depth for the four lowest level crossings in the band picture corresponding to the four lowest Bragg diffraction orders. (b) The corresponding variation of Ω_D/Ω_R . The behavior of (c) Ω_D and (d) Ω_R for large lattice depths.

the observation of reduced diffraction efficiency (see green curves corresponding to the shortest pulses for $N_B = 1–4$ in Fig. 6)—a straightforward experimental diagnostic—making the Bloch-band picture ideally suited for light pulse atom diffraction and interferometry. As expected, adiabaticity is restored for larger N_B with the peak diffracted fraction for the shortest pulses calculated by numerical integration in the free-particle basis (dashed green lines) reaching 0.92, 0.97, and 0.99 for $N_B = 8, 12$, and 16, respectively [the $N_B = 16$ case is shown in Figs. 6(e) and 6(j)].

APPENDIX B: FULL NUMERICAL INTEGRATION

For the full numerical simulation, we project onto a momentum-space basis $\{\dots, |2\hbar k, g\rangle, |\hbar k, e\rangle, |0\hbar k, g\rangle, |-\hbar k, e\rangle, |-2\hbar k, g\rangle\dots\}$, where the minimum and maximum momenta are chosen by testing for convergence. For the purposes of this discussion, we truncate to five states [34]. While this basis contains both ground and electronically excited states, we find that the results do not depend on the detuning, Δ , of the diffraction beams from the ground to excited state resonance, so long as the same two-photon Rabi frequency [$\omega_R^2/(2\Delta)$] is used. Utilizing the rotating frame approximation and transforming to the dressed-state basis gives a Hamiltonian of the form

$$\begin{pmatrix} 4\hbar\omega_{\text{rec}} & \frac{\hbar\omega_R}{2} & 0 & 0 & 0 \\ \frac{\hbar\omega_R}{2} & \hbar\omega_{\text{rec}} - \hbar\Delta & \frac{\hbar\omega_R}{2} & 0 & 0 \\ 0 & \frac{\hbar\omega_R}{2} & 0 & \frac{\hbar\omega_R}{2} & 0 \\ 0 & 0 & \frac{\hbar\omega_R}{2} & \hbar\omega_{\text{rec}} - \hbar\Delta & \frac{\hbar\omega_R}{2} \\ 0 & 0 & 0 & \frac{\hbar\omega_R}{2} & 4\hbar\omega_{\text{rec}} \end{pmatrix}.$$

We numerically integrate to obtain the time evolution operator \hat{U} for the full diffraction pulse and then extract the diffraction phase as the phase of the transition matrix element between two states of opposite momentum. For example, to simulate an $N = 2$ pulse, the phase of the matrix element $\langle 2\hbar k, g | \hat{U} | -2\hbar k, g \rangle$ is compared to the phase of $\langle 0\hbar k, g | \hat{U} | 0\hbar k, g \rangle$, as would be the case in an interferometer. For extracting the diffraction phase of a single state we compare to a much higher momentum state (e.g., 16 $\hbar k$ higher momentum), which should have negligible diffraction phase, and then confirm that neighboring high-momentum states give the same results. This removes effects from momentum-independent ac Stark shifts.

APPENDIX C: PERTURBATIVE SCALINGS FOR DIFFRACTION PHASE AND DEEP LATTICES

The behavior of the diffraction phase can be straightforwardly determined analytically in the limit of low lattice depth. Here, Ω_R can be taken to be the RHS of Eq. (1) in the main text, which is inversely proportional to the

π -pulse time. Ω_D is determined in second-order perturbation by the first (two-photon) off-resonant transition. For $N_B > 1$, $\Omega_D \propto (\frac{\omega_R^2}{\Delta})^2 \frac{1}{N_B \omega_{\text{rec}}} = \frac{(U_0/\hbar)^2}{N_B \omega_{\text{rec}}}$. For the simple case of square pulses, $\Phi_D \propto \frac{\Omega_D}{\Omega_R}$, and this proportionality also indicates the behavior of Φ_D for a general pulse shape, with appropriate integration over the temporal profile of the diffraction pulse. Thus, $\Phi_D \propto \frac{\Omega_D}{\Omega_R} \propto \frac{1}{N_B} (\frac{U_0/\hbar}{\omega_{\text{rec}}})^{2-N_B}$. Ω_D is negative for $N_B = 1$, and $\Phi_D \propto -\frac{1}{N_B} (\frac{U_0/\hbar}{\omega_{\text{rec}}})^{2-N_B}$. This behavior can be seen in the weak lattice limit of the curves in Figs. 7(a) and 7(b).

At larger lattice depth, the behavior deviates significantly from the perturbative expressions with Ω_D exhibiting a local maximum for all Bragg processes except $N_B = 1$ [see Fig. 7(c)]. The locations of these maxima are in the diabatic regime for Bragg π -pulses.

The deep lattice behavior of the Rabi frequencies or band gaps is shown in Fig. 7(d). We note that in the limit of large lattice depth, the Rabi frequencies of all Bragg orders approach the values for the band gaps in the tight-binding limit corresponding to the harmonic oscillator spacing of $2\sqrt{U_0\omega_{\text{rec}}/\hbar}$.

[1] F. Bloch, *Z. Phys.* **52**, 555 (1928).

[2] N. Ashcroft and N. Mermin, *Solid State Physics* (Harcourt College Publishers, Orlando, 1976).

[3] I. Bloch, J. Dalibard, and W. Zwerger, *Rev. Mod. Phys.* **80**, 885 (2008).

[4] I. Bloch, J. Dalibard, and S. Nascimbene, *Nat. Phys.* **8**, 267 (2012).

[5] S. Kuhr, *Nat. Sci. Rev.* **3**, 170 (2016).

[6] G. Tino and M. Kasevich, Atom Interferometry, *Proceedings of the International School of Physics “Enrico Fermi”, Course 188* (IOS Press, Washington, DC, 2014).

[7] J. M. McGuirk, G. T. Foster, J. B. Fixler, M. J. Snadden, and M. A. Kasevich, *Phys. Rev. A* **65**, 033608 (2002).

[8] D. S. Durfee, Y. K. Shaham, and M. A. Kasevich, *Phys. Rev. Lett.* **97**, 240801 (2006).

[9] I. Dutta, D. Savoie, B. Fang, B. Venon, C. L. Garrido Alzar, R. Geiger, and A. Landragin, *Phys. Rev. Lett.* **116**, 183003 (2016).

[10] R. Geiger, V. Ménoret, G. Stern, N. Zahzam, P. Cheinet, B. Battelier, A. Villing, F. Moron, M. Lours, Y. Bidel *et al.*, *Nat. Commun.* **2**, 474 (2011).

[11] S. Fray, C. A. Diez, T. W. Hänsch, and M. Weitz, *Phys. Rev. Lett.* **93**, 240404 (2004).

[12] D. Schlippert, J. Hartwig, H. Albers, L. L. Richardson, C. Schubert, A. Roura, W. P. Schleich, W. Ertmer, and E. M. Rasel, *Phys. Rev. Lett.* **112**, 203002 (2014).

[13] M. G. Tarallo, T. Mazzoni, N. Poli, D. V. Sutyrin, X. Zhang, and G. M. Tino, *Phys. Rev. Lett.* **113**, 023005 (2014).

[14] R. Bouchendira, P. Cladé, S. Guellati-Khélifa, F. Nez, and F. Biraben, *Phys. Rev. Lett.* **106**, 080801 (2011).

[15] R. H. Parker, C. Yu, B. Estey, W. Zhong, and H. Müller, *Science* **360**, 191 (2018).

[16] D. M. Giltner, R. W. McGowan, and S. A. Lee, *Phys. Rev. A* **52**, 3966 (1995).

[17] S. Gupta, A. E. Leanhardt, A. D. Cronin, and D. E. Pritchard, *Cr. Acad. Sci. IV-Phys.* **2**, 479 (2001).

[18] S. Durr and G. Rempe, *Phys. Rev. A* **59**, 1495 (1999).

[19] M. Horne, I. Jex, and A. Zeilinger, *Phys. Rev. A* **59**, 2190 (1999).

[20] H. Müller, S.-W. Chiow, and S. Chu, *Phys. Rev. A* **77**, 023609 (2008).

[21] C. Champenois, M. Büchner, R. Delhuille, C. Mathevet, C. Robilliard, C. Rizzo, and J. Vigué, *Eur. Phys. J. D.* **13**, 271 (2001).

[22] M. Büchner, R. Delhuille, A. Miffre, C. Robilliard, J. Vigué, and C. Champenois, *Phys. Rev. A* **68**, 013607 (2003).

[23] B. Plotkin-Swing, D. Gochnauer, K. E. McAlpine, E. S. Cooper, A. O. Jamison, and S. Gupta, *Phys. Rev. Lett.* **121**, 133201 (2018).

[24] M. A. H. M. Jansen, K. F. E. M. Domen, H. C. W. Beijerinck, and K. A. H. van Leeuwen, *Phys. Rev. A* **76**, 053629 (2007).

[25] T. Mazzoni, X. Zhang, R. Del Aguila, L. Salvi, N. Poli, and G. M. Tino, *Phys. Rev. A* **92**, 053619 (2015).

[26] Q. Hu, J. Yang, Y. Luo, A. Jia, C. Wei, and Z. Li, *Optik (Munich, Ger.)* **131**, 632 (2017).

[27] A. O. Jamison, B. Plotkin-Swing, and S. Gupta, *Phys. Rev. A* **90**, 063606 (2014).

[28] B. Estey, C. Yu, H. Müller, P.-C. Kuan, and S.-Y. Lan, *Phys. Rev. Lett.* **115**, 083002 (2015).

[29] S. W. Chiow, T. Kovachy, H. C. Chien, and M. A. Kasevich, *Phys. Rev. Lett.* **107**, 130403 (2011).

[30] When $q = 0$, the outer paths are in a symmetric or antisymmetric superposition of the seventh and eighth bands. In this case, an eighth-order Bragg resonance condition is met for the outer paths. However, Ω_R and Ω_D are very small for this $N_B = 8$ process, making any population transfer or diffraction phase contributions negligible. Even at the largest values shown of 10 rad at 34 recoils in Fig. 5(b), the population transfer for $N_B = 8$ is $<10^{-4}$ and the diffraction phase from outer paths <0.1 rad.

- [31] S. Kling, T. Salger, C. Grossert, and M. Weitz, *Phys. Rev. Lett.* **105**, 215301 (2010).
- [32] Z. A. Geiger, K. M. Fujiwara, K. Singh, R. Senaratne, S. V. Rajagopal, M. Lipatov, T. Shimasaki, R. Driben, V. V. Konotop, T. Meier, and D. M. Weld, *Phys. Rev. Lett.* **120**, 213201 (2018).
- [33] C. J. Fujiwara, K. Singh, Z. A. Geiger, R. Senaratne, S. V. Rajagopal, M. Lipatov, and D. M. Weld, *Phys. Rev. Lett.* **122**, 010402 (2019).
- [34] In practice, we find 17 states to be necessary for sufficient accuracy in modeling our second-order Bragg mirror pulses.